ACS APPLIED MATERIALS & INTERFACES

Letter

www.acsami.org

Chemical Conversion Synthesis of ZnS Shell on ZnO Nanowire Arrays: Morphology Evolution and Its Effect on Dye-Sensitized Solar Cell

Lizhu Liu, Yiqing Chen,* Taibo Guo, Yunqing Zhu, Yong Su, Chong Jia, Meiqin Wei, and Yinfen Cheng

School of Materials Science and Engineering, Hefei University of Technology, Hefei, Anhui 230009, People's Republic of China

Supporting Information

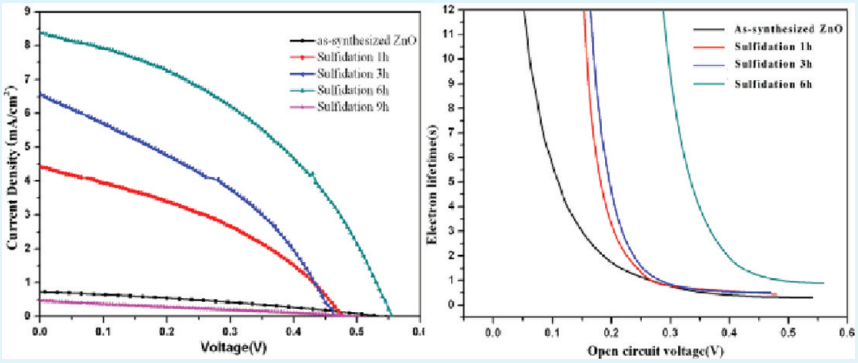

ABSTRACT: Heterostructured ZnO/ZnS core/shell nanowire arrays have been successfully fabricated to serve as photoanode for the dye-sensitized solar cells (DSSCs) by a facile two-step approach, combining hydrothermal deposition and liquid-phase chemical conversion process. The morphology evolution of the ZnS coated on the ZnO nanowires and its effect on the performance of the DSSCs were systematically investigated by varying the reaction time during the chemical conversion process. The results show that the compact ZnS shell can effectively promote the photogenerated electrons transfer from the excited dye molecules to the conduction band of the ZnO, simultaneously suppress the recombination for the injected elelctrons from the dye and the redox electrolyte. As reaction time goes by, the surface of the nanowires becomes coarse because of the newly formed ZnS nanoparticles, which will enhance the dye loading, resulting in increment of the short-circuit current density (J_{SC}) . Open-circuit photovoltage decay measurements also show that the electron lifetime (τ_n) in the ZnO/ZnS core/shell nanostructures can be significantly prolonged because of the lower surface trap density in the ZnO after ZnS coating. For the ZnO/ZnS core/shell nanostructures, the J_{SC} and η can reach a maximum of 8.38 mA/cm^2 and 1.92% after 6 h conversion time, corresponding to 12- and 16-fold increments of as-synthesized ZnO, respectively.

KEYWORDS: *ZnO-ZnS, dye-sensitized solar cell, core−shell nanostructure, nanowire arrays, liquid-phase chemical conversion, type II band alignment*

1. INTRODUCTION

Dye-sensitized solar cells (DSSCs) are of great interest as a new generation of photovoltaic devices because of its low fabrication cost, easy manufacturing process, and environmental friendship.[1,2] As one of the key components of the DSSCs, the photoanode, composed of nanocrystalline semiconductor materials, has significant influence on the photovoltaic performance and becomes a critical issue in cell design.[3,4] With large surface areas for loading the light-harvesting dye molecules, TiO_2, ZnO, and SnO_2 nanoparticles films were predominantly used as anode materials for DSSCs. However, the nanoparticles based DSSCs often face restriction of the trap-limited diffusion process at grain boundary and the nanoparticles/electrolyte interface. As a result, a short electron diffusion length will increase the recombination probability of the electrons with redox species, which is detrimental to the device performance.[5,6] In this regard, one dimension (1D) ZnO nanostructures are emerging as an alternative to nanocrystalline films for solar cell applications, as the aim is expected to increase the electron diffusion length by providing a direct pathway for rapid charge collection to decrease the charge recombination rate.[7,8] Moreover, the well-aligned ZnO nanostructure can be easily fabricated and its morphology can be modified. Unfortunately, the dye loading on the 1 D ZnO is often insufficient because of its relatively large particle size and small surface area. And the competition between the generation and recombination of the photoexcited carriers in 1D ZnO DSSCs is still a main bottleneck for improving overall solar cell performance. For instance, ZnO has a relative chemical instability in acid dye and readily reacts with dye molecules

Received: October 17, 2011
Accepted: December 12, 2011
Published: December 12, 2011

   dx.doi.org/10.1021/am201425n | ACS Appl. Mater. Interfaces 2012, 4, 17–23

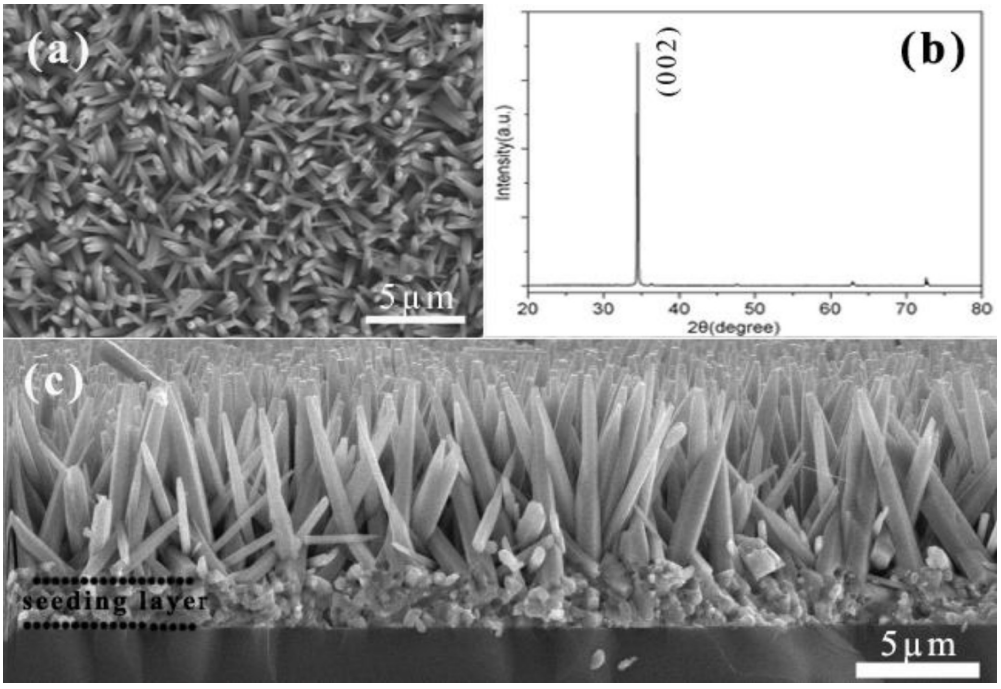

Figure 1. (a) Top-view SEM image of the as-synthesized ZnO nanowire arrays. (b) Corresponding XRD pattern. (c) Side-view SEM image of the as-synthesized ZnO nanowire arrays on an FTO substrate.

to form insulating [dye-Zn^{2+}] complexes, which may hinder electron injection into ZnO from the dye molecules and cause a decrease in J_{SC}.[9] On the other hand, photogenerated electrons can recombine with dye or redox electrolyte and decrease the current density in bared ZnO nanowires photoanode, thereby reducing the cell efficiency.[6] So, introducing a protective layer on the ZnO and simultaneous increasing the surface area by surface treatment should be a promising approach to improve the performance of DSSCs.

A number of advantages have been demonstrated for ZnO/ZnS core/shell nanocable architectures, where charge separation of the electron and hole is often facilitated by type II band alignment of ZnO/ZnS core/shell heterostructures at the interface of the two different materials.[10−17] Due to a higher band gap of ZnS shell, the excited electrons are confined inside the ZnO and the holes are localized in ZnS shell. In addition, introducing of ZnS layer between the ZnO and dye molecules can effectively avoid the formation of the insulating [dye-Zn^{2+}] complexes, which is beneficial to improve the device stability and electron injection. Up to now, several methods have been reported to fabricate ZnO/ZnS core/shell nanowires including vapor deposition approach,[11] chemical bath deposition,[16] and template method.[17] However, the methods mentioned above generally require high reaction temperature, tedious processes, complex equipments or templates, etc. Meanwhile, the morphology of heterostructures cannot be controlled easily and the compositions are difficult to be modulated precisely. In addition, the synthesized ZnS shells are mostly polycrystalline. Recently, chemical conversion process and cation exchange have been demonstrated as a facile and effective method to fabricate the ZnO/ZnS heterostructure.[10,15]

In the present work, we demonstrate the successful fabrication of ZnO/ZnS core/shell heterostructure by a facile two-step approach combining hydrothermal deposition and liquid-phase chemical conversion process. The single-crystal ZnS shell was formed in the chemical conversion process. By varying the chemical reaction time, we made a systematic investigation on the morphology evolution of the ZnS shell and its influence on the photovoltaic properties of ZnO/ZnS core/shell based DSSCs. The synthesized ZnS layers can effectively reduce the charge recombination of photogenerated electrons with the oxidized species in the electrolyte and oxidized dye molecules. And the compact ZnS shell with coarse surface can also enlarge the internal surface area to absorb more dye molecules, resulting in increment of the short-circuit current density.

2. EXPERIMENTAL SECTION

2.1. Synthesis of ZnO Nanowire Arrays. The samples were prepared by a two-step method including substrate pretreatment and hydrothermal process. First, a ZnO seed layer was formed on the fluorine-doped tin oxide (FTO) glass (Nippon Sheet Glass Co., Ltd., R_s = 15 ohm/sq) using a dip-coating method, similar with that reported earlier.[18] Then, the substrate was suspended face-down in the aqueous solution of 0.05 M zinc nitrate hexahydrate and 0.05 M hexamethylenetetramine and heated at 90 °C for 6 h. Finally, the substrate with product was rinsed with deionized water and annealed in air at 450 °C for 3 h to remove residual surface salts.

2.2. Synthesis of ZnO/ZnS Core/Shell Structured Nanowire Arrays. A simple chemical conversion approach was adopted to fabricate ZnO/ZnS core/shell nanostructures. The substrate with ZnO nanowire arrays was immersed in thiacetamide (TAA) aqueous solution (0.2 M) and the sulfidation process was carried out at 90 °C for a period of time. The final product was also washed with deionized water repeatedly to remove the impurities and dried at room temperature.

2.3. Cell Fabrication. For DSSCs fabrication, ZnO nanowire arrays with and without ZnS shell as electrodes were immersed in a 0.3 × 10^{-3} mol L^{-1} ethanol solution of N719 (Dalian HeptaChroma SolarTech) for 2 h. The DSSCs

were assembled by sandwiching the (FTO)/(dye-sensitized nanowire arrays photoanode)/(Pt-coated FTO cathode) using a piece of hot melt Surlyn (Dalian HeptaChroma SolarTech, 25 μm thick) as a spacer. The internal space of the cell was filled with an electrolyte (Dalian HeptaChroma SolarTech, 0.5 M LiI, 50 mM I_2, 0.5 M 4-tertbutylpyridine in 3-methoxypropionitrile) by capillary action through a small predrilled hole in the counter electrode. The total active electrode area is 0.5 cm^2.

2.4. Characterization. The synthesized ZnO nanowire arrays were characterized by X-ray diffraction (XRD, D/MaxrB). The morphologies of the nanowires were characterized by field emission scanning electron microscopy (FESEM: S-4700, Hitachi, operating voltage: 10 kV) and high-resolution transmission electron microscopy (HRTEM; JEOL-2010). Energy dispersive X-ray spectroscopy (EDS) and the selected area electron diffraction (SAED) were processed during HRTEM measurements. The formation of ZnS on the ZnO nanowires and the bonding characteristics were determined by X-ray photoelectron spectroscopy (XPS, ESCALAB 250). UV−vis absorption spectra were recorded on a DUV-3700 spectrophotometer. The photoluminescence (PL) spectra were measured at room temperature with a He−Cd laser (325 nm) as the excitation source. The photovoltaic performance of the DSCCs were measured by KEITHLEY 4200 under solar simulator (XES-301S, Xenon lamp, AM 1.5, 100 mW cm^{-2}), and the incident light intensity was calibrated with a standard crystalline silicon solar cell.

3. RESULTS AND DISCUSSION

The morphology and crystalline structure of the as-synthesized ZnO nanowire arrays are shown in Figure 1. The top-view (Figure 1a) shows that the nanowire arrays have been successfully prepared with the uniform and compact distribution on the FTO substrate. The side-view (Figure 1c) clearly shows that the nanowires have smooth surface with the average diameter of about 200 nm and the length of about 5 μm. As shown in the corresponding XRD pattern (Figure 1b), the sample has a hexagonal wurtzite structure (JCPDS 36−1451) with preferential orientation along the *c* axis. The strong and sharp (002) diffraction peak also indicates that the nanowire arrays have a narrow size distribution and good crystallinity, which is beneficial to provide fast transport for the photogenerated electrons through the nanowires to the FTO layer. In addition, all wires are separated at the foot of the array and no clear fusion can be observed. The nanowires fusing with each other at the foot will result in a loss of surface area for dye adsorption.

To make the conversion of ZnO nanowire to ZnO/ZnS core/shell nanostructure, the FTO with the as-synthesized ZnO nanowire arrays was transferred into a solution containing 0.2 M TAA. In the reaction system, the TAA hydrolyzes and provides sulfide ions (S^{2-}) at 90 °C. Then S^{2-} will react with the Zn^{2+} slowly dissolved from the surface of ZnO nanowire to form ZnS nanopaticles. Figure 2 is the SEM images presenting the morphology evolution of the samples during the chemical conversion process. The well-ordered nanowires still exist (Figure 2a−c′), suggesting that conversion process cannot damage the arrays as long as 6 h. Different from the as-synthesized ZnO, the surface morphology of the sample becomes coarse after sulfidation 1 h, and nanoparticles distribute sparsely on the surface of the nanowires, as shown in Figure 2a′. Further extending the sulfidation time (3 h), the surface roughness of the product increases and the nanoparticles completely cover on the ZnO nanowires (Figure 2b, b′). As the sulfidation time is increased to 6 h, more nanoparticles pile up on the initial shell which is robust enough to form a coaxial core/shell structure, indicated by arrows in the Figure 2c. However, when further prolonging the sulfidation time to 9 h, the arrays collapse (Figure 2d) and nanowires are converted into nanotubes, as can be clearly seen from the damaged top-open ended nanotubes in Figure 2d′.

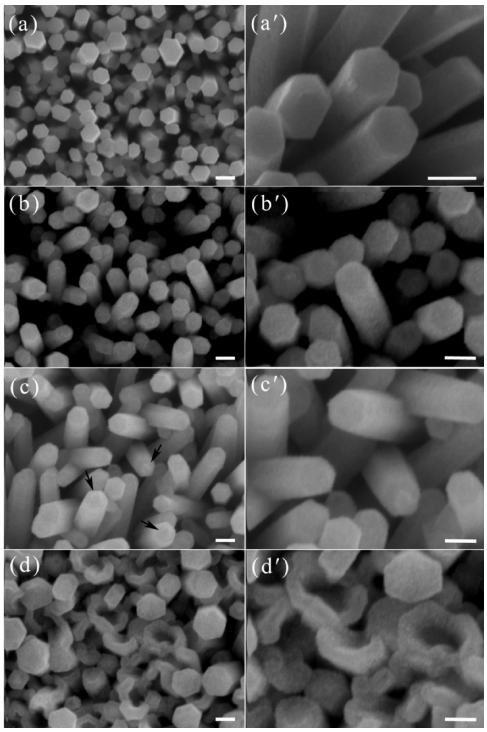

Figure 2. SEM images of the products for different sulfidation time: (a) 1, (b) 3, (c) 6, and (d) 9 h. (a′−d′) Corresponding magnified SEM images. Scale bar 200 nm.

To confirm the formation of the ZnS shell on the ZnO nanowires, we performed XPS measurement. Figure 3a is the XPS spectrum in which Zn, O, S and C peaks can be observed. The S peaks detected in XPS indicate that the new layer contains sulfur in the sulfidation process. The peak appears at 521.5 eV is ascribed to the lattice oxygen in the ZnO/ZnS structure.[19] The spectrum in Figure 3c shows the S2p3/2 and S2p1/2 peaks, located at 161.6 and 162.8 eV, respectively, are related to Zn−S bondings,[20] suggesting that ZnS was successfully synthesized through the chemical conversion process in our experiments. The $Zn2p_{3/2}$ and $Zn2p_{1/2}$ peaks are also shown in Figure 3d. Therefore, the XPS spectra confirm that ZnO on the surface of nanowire is etched and converted into ZnS, resulting in formation of the ZnO/ZnS core/shell heterostructure.

HRTEM observation can give further insight into the morphologies and microstructures of the products for the different sulfidation time. The typical images of the products, obtained for sulfidation 1 h, are shown in Figure 4. The great difference in contrast between the edge and center indicates the formation of core/shell structure. And the ZnS shell is uniform in width with the thickness about 30 nm. The SAED pattern of ZnO core (bottom-left inset of Figure 4a) shows that ZnO nanowires grow along [0001] direction, which is consistent with that in XRD observation. The bright spots in SAED pattern (top-right inset of Figure 4a), recorded from ZnS shell,

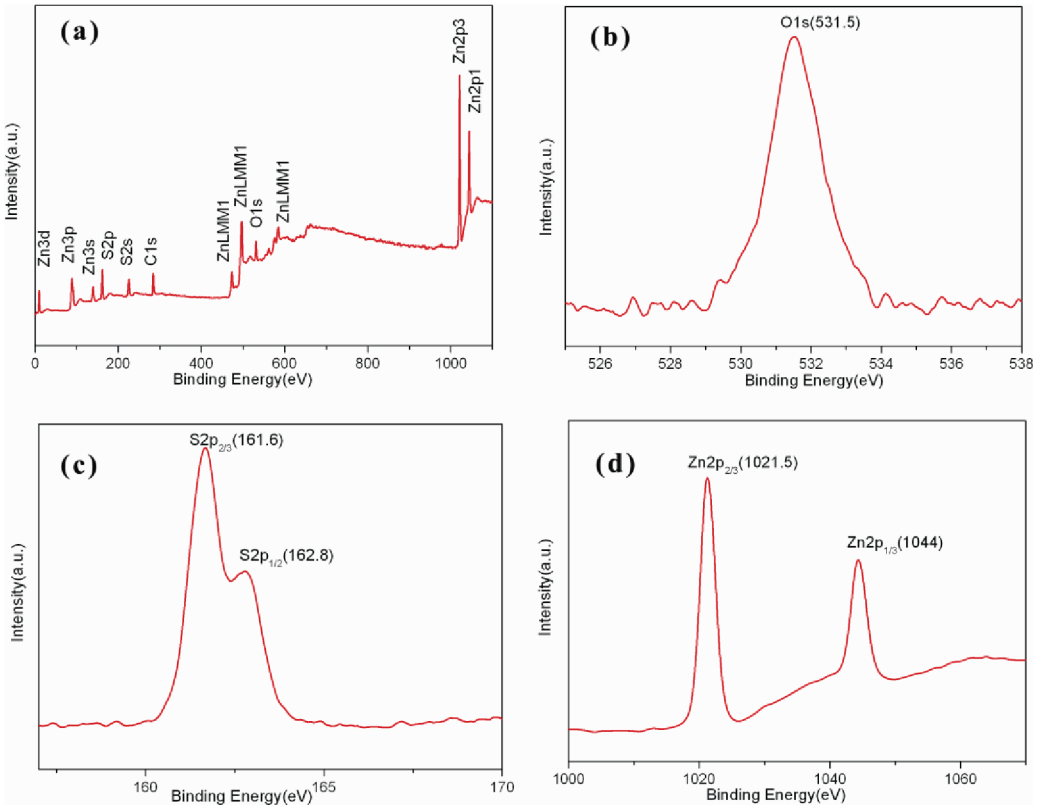

Figure 3. XPS spectra of ZnO/ZnS core/shell heterostructure: (a) complete survey and (b) O1s, (c) S2p, and (d) Zn2p peaks.

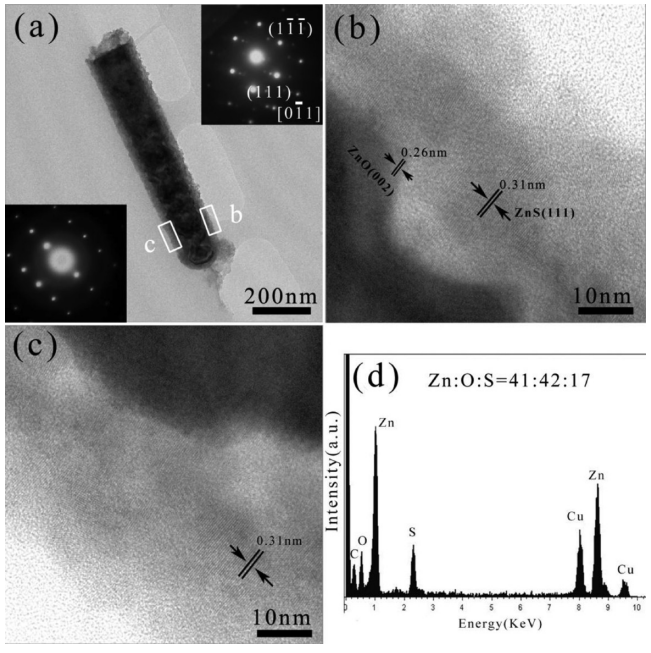

Figure 4. (a) TEM image of the products for sulfidation 1 h. The bottom-left and top-right insets give the corresponding selected area electron diffraction (SAED) patterns for core and shell of nanowire, respectively. (b, c) HRTEM images taken at the edges of ZnS shell. (d) EDS spectrum of the nanowire.

and crystal lattice fringes (about 0.31 nm, shown in Figure 4b, c) both prove its crystal nature, which is different from the polycrystalline ZnS films reported before.[10,12,17] The marked interplannar *d* spacings of 0.26 and 0.31 nm correspond, respectively, to the (0002) lattice plane of ZnO with the $[2\bar{1}\bar{1}0]$ zone axis and the (111) lattice plane of ZnS with the $[0\bar{1}1]$ zone axis.[26] Thus, the core and shell have an epitaxial growth with the growth relationship of $[0001]_{ZnO}\|[111]_{ZnS}$. From the compositional information of the EDS spectrum in Figure 4d, S element is found to be present along with Zn and O, with atom ratio of Zn, O, and S about 41:42:17, providing powerful evidence that S element is successfully incorporated into the ZnO nanowire at the surface level. Some Cu and C signals were also detected, which result from the TEM grid. Figure 5 shows the representative HRTEM images of the products obtained for sulfidation 6 h, where the core/shell structure can be also observed. Compared with the ZnS shell obtained at 1 h, the ZnS shell is thicker (about 50 nm) and becomes quite coarse, indicated by arrows in the Figure 5a. The HRTEM images taken on the surface of ZnS shell are shown in Figure 5b and 5c. As displayed in Figure 5b, the zigzag edge of the shell can improve its roughness, which results in the enhancement of the dye loading as well as the decrease in the reflection of the incident light so as to increase the current density in DSSCs.[10] One can notice that the compact ZnS shell is covered by many different sized ZnS nanoparticles (Figure 5c) and larger nanoparticles are also found on the surface of the ZnS nanotubes obtained for 9 h sulfidation time (see the Supporting Information, Figure S1). As shown is Figure 5d, S/O atom ratio becomes much higher than that in Figure 4d, which means that more and more ZnO were converted into ZnS with the increase in sulfidation reaction time.

To investigate the effects of ZnO/ZnS core/shell heterostructures on the DSSCs performance, we fabricated a batch of DSSCs using ZnO nanowires and ZnO/ZnS core/shell nanowire arrays obtained at different stages of the conversion process. The photocurrent density−voltage characteristics are

dx.doi.org/10.1021/am201425n | *ACS Appl. Mater. Interfaces* 2012, 4, 17−23

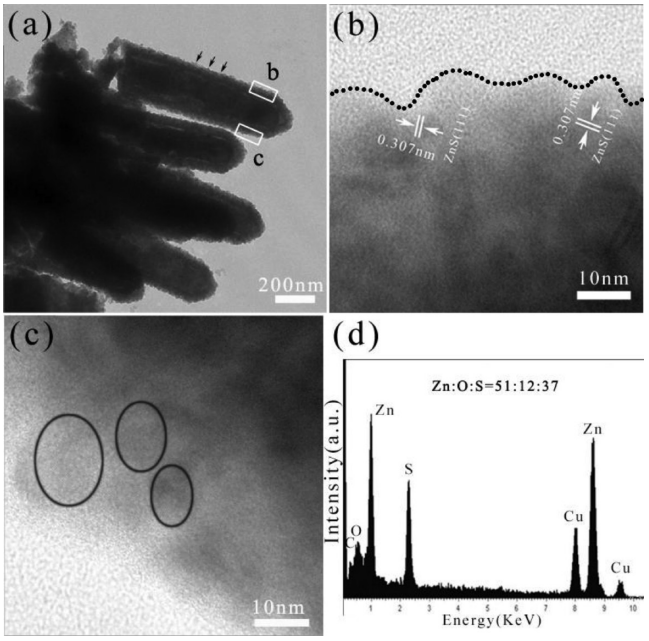

Figure 5. (a) TEM image of the products for sulfidation 6 h. (b, c) HRTEM images taken at the edges of ZnS shell. (d) EDS spectrum of the nanowire.

shown in Figure 6 and corresponding photovoltaic parameters of the DSSCs are summarized in Table 1. For the as-

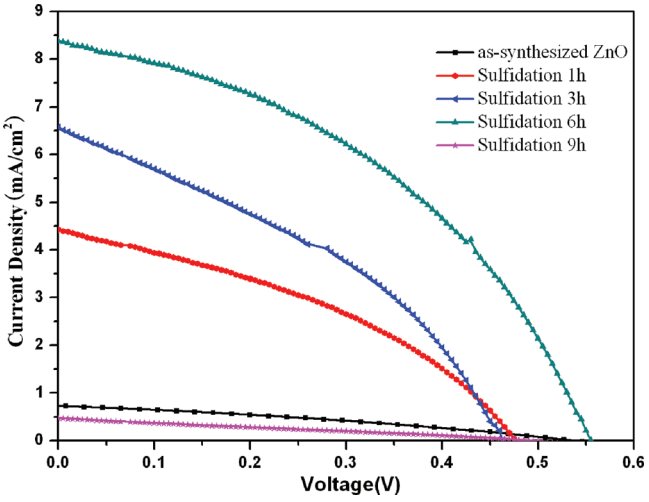

Figure 6. *I*–*V* characteristics of the solar cells fabricated with as-synthesized ZnO nanowires arrays and ZnO/ZnO core/shell nanostructures for different sulfidation time.

synthesized ZnO nanowire arrays, a short-circuit current (J_{SC}) of 0.671 mA/cm^2 and an overall power conversion efficiency (η) of 0.12% are achieved, whereas for the ZnO/ZnS core/shell nanostructures after sulfidation 1 h, the J_{SC} and η can be improved to 4.42 mA/cm^2 and 0.82%. Both J_{SC} and η are significantly improved as the reaction time increases. For ZnO/ZnS core/shell nanostructures, the J_{SC} and η values can reach a maximum of 8.38 mA/cm^2 and 1.92% after sulfidation for 6 h, corresponding to 12- and 16-fold increments of as-synthesized ZnO, respectively. No significant change in open-circuit voltage (V_{OC}) and fill factor (FF) happen after coating ZnS on the ZnO nanowire. Therefore, it can be concluded that ZnO/ZnS heterostructure increases the overall solar cell performance mainly by increasing the J_{SC}.

The recombination process of the electrons injected into the conduction band (CB) of ZnO with either the dye or the redox electrolyte is considered as one of the most important factors to determine the short-circuit current density in the anode materials for DSSCs.[6,9] When ZnO is stacked with other environmental benign and abundant functional semiconductor materials such as ZnS, the lattice strain will exist along the interface of type II ZnO/ZnS heterostructure. The interface strain can lead to an increase in the oscillator strength, where the individual band gap could be smaller than the initial value.[13,14] As demonstrated in Scheme 1, the band gap of ZnO

Scheme 1. Energy Levels of ZnO before and after Coating ZnS

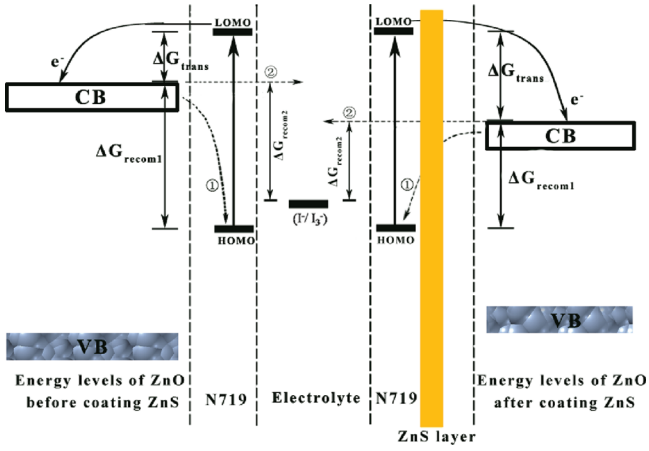

can be compressed induced by the interface strain from such a staggered II band alignment for ZnO/ZnS heterostructure. In the thermodynamic point of view, the free energy change (ΔG) for the electron transfer from the excited dye molecules to the CB of ZnS coated ZnO ($\Delta G_{transfer}$) is more positive than that of uncoated ZnO, meanwhile, the free energy changes for recombination (including ΔG_{recom1} and ΔG_{recom2}) for coated ZnO is less positive than that of uncoated ZnO. As a result, the increased $\Delta G_{transfer}$ is beneficial to charge transfer from the excited molecules to the CB while charge recombination process is inhibited. Therefore, the ZnS coating on the ZnO

Table 1. Photovoltaic Performances of ZnO-Based DSSCs

electrode	V_{OC} (V)	J_{SC} (mA cm^{-2})	FF (%)	η (%)
as-synthesized ZnO	0.542 ± 0.001	0.671 ± 0.004	34.3 ± 0.1	0.12 ± 0.04
sulfidation 1 h	0.481 ± 0.003	4.42 ± 0.02	38.2 ± 0.3	0.82 ± 0.04
sulfidation 3 h	0.470 ± 0.004	6.57 ± 0.01	37.4 ± 0.1	1.14 ± 0.03
sulfidation 6 h	0.564 ± 0.001	8.38 ± 0.01	41.6 ± 0.2	1.92 ± 0.03
sulfidation 9 h	0.462 ± 0.001	0.474 ± 0.004	28.2 ± 0.4	0.06 ± 0.04

dx.doi.org/10.1021/am201425n | ACS Appl. Mater. Interfaces 2012, 4, 17–23

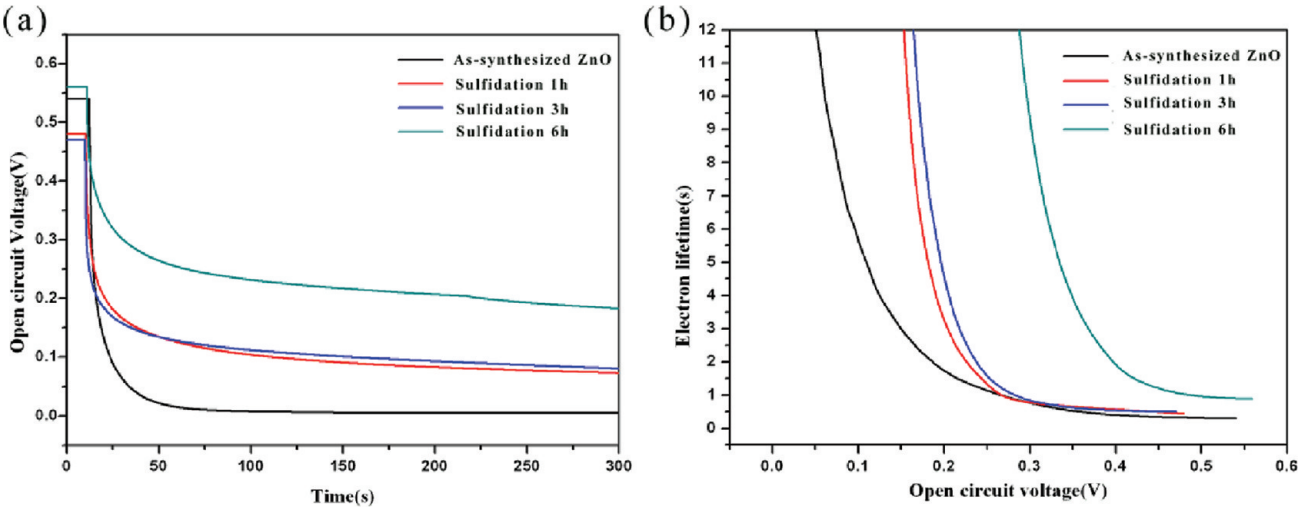

Figure 7. Open-circuit voltage−decay curve and measured electron lifetime in as-synthesized ZnO nanowire arrays and ZnO/ZnO core/shell nanostructures for different sulfidation time. (a) Voltage−decay measurement. (b) Electron lifetime derived from equation as a function of V_{OC}.

can retard charge recombination process effectively, and significantly increase the current density in the photoanode materials. Moreover, because the higher axial interface strain from the thick ZnS layer would lead to larger band offset,[25] the current density should be enhanced along with the sulfidation time.

To further understand the effect of ZnS shell on current density of the ZnO photoanode, we investigated the electron recombination kinetics of these two types of DSSCs with and without ZnS coating. As a powerful tool, the transient V_{OC} as a function of time upon turning off the illumination can be used to study the electron recombination kinetics of the DSSCs.[21]The electron lifetime (τ_n) is mainly affected by the surface state traps of the phtotoanode materials.[16] In the room-temperature PL spectra of the ZnO and ZnS core/shell nanostructures (see the Supporting Information, Figure S2), the visible emission, attributed to the oxygen vacancies in the ZnO surface, is reduced obviously. The lower surface trap density for the photoanode often represents a higher electron lifetime.[16] Figure 7 plots the V_{OC} decay as a function of time measured using ZnO nanowires and ZnO/ZnS core/shell nanowires for different sulfidation time. From Figure 7a, it can be clearly seen that the DSSCs based on ZnO/ZnS core/shell photoanodes have significantly slower V_{OC} decay rate than that based on as-synthesized ZnO nanowires, indicating slow recombination kinetics in ZnO/ZnS core/shell photoanodes. The lifetime of photogenerated electrons surviving recombination, can be determined from the V_{OC} decay rate by the following equation[21,22]

$$\tau_n = -(k_B T/e)(dV_{oc}/dt)^{-1}$$

where $k_B = 1.38 \times 10^{-23}$ J/K is Boltzmann constant and T is absolute temperature. The calculated τ_n is shown in Figure 7b as a function of V_{OC} for the same photoanodes above. It can be observed that τ_n of the ZnO/ZnS core/shell photoanodes are longer than that of as-synthesized ZnO photoanode. At V_{OC}, which is the maximum voltage of the DSSC, τ_n for as-synthesized ZnO photoanode is about 0.3 s. After sulfidation for 1 and 3 h, τ_n is increased to 0.44 and 0.5 s, respectively. As the sulfidation time is increased to 6 h, τ_n extends to 0.9 s, which is much higher than that of ZnO nanowires-based photoanodes reported before.[22,23] So, the formation of the ZnS shell can reduce surface trap density, and effectively suppress the electron recombination.

The volume of dye molecules attached to the photoanode is also thought to associate with the short-circuit current density.[24] Enlargement of internal surface area within the photoanode can absorb more dye molecules, resulting in increment of the short-circuit current density.[10] The optical absorption spectra of the samples sensitized by N719 dye are shown in Figure 8. It can be clearly seen that the absorption

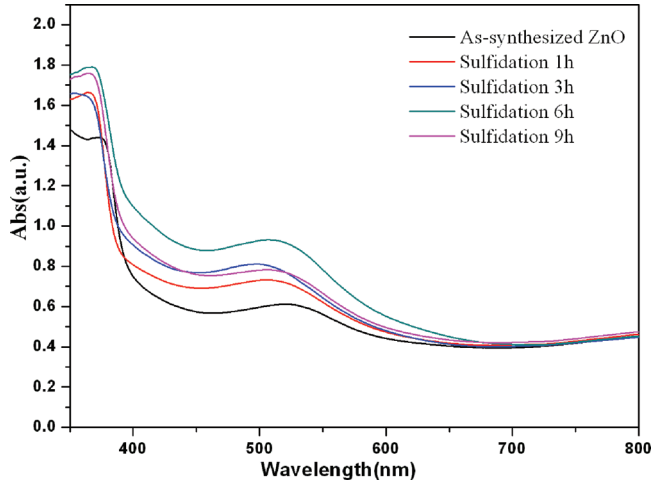

Figure 8. UV−vis absorption spectra of the samples sensitized by N719 dye.

centered around 510 nm, originating from the dye molecules, is larger for the ZnO/ZnS core/shell nanostructures than for the bare ZnO nanowires. For the ZnO/ZnS core/shell nanostructures, as sulfidation time goes by, the absorption can be increased. From the SEM and HRTEM observations, extending the sulfidation time, the surface of the nanowires becomes coarse due to the new formed ZnS nanoparticles, which would enhance the dye loading as well as decrease the reflection of the incident light so as to increase the current density in DSSCs. The photoanode obtained under 6 h sulfidation time has the highest absorption, resulting distinguished short-circuit current density and energy conversion efficiency, indicating that ZnO

dx.doi.org/10.1021/am201425n | ACS Appl. Mater. Interfaces 2012, 4, 17−23

possessing compact ZnS shell and high surface roughness should be an ideal photoanode structure for the ZnO/ZnS core/shell based DSSCs.

4. CONCLUSION

In summary, ZnO/ZnS core/shell heterostructures have been fabricated to serve as the photoanode of DSSCs via a facile two-step approach combining hydrothermal deposition and liquid-phase chemical conversion process. Morphology and component of the products can be easily controlled by the sulfidation time. The systematic investigations were made on the influence of ZnS shell on the photovoltaic properties of ZnO-based DSSCs. The J_{SC} and η are significantly improved for the ZnO/ZnS core/shell photoanodes compared with as-synthesized ZnO photoanode. The improvement can be explained in association with increasing the dye loading and preventing the charge recombination of photogenerated electrons with the oxidized species in the electrolyte and oxidized dye molecules after ZnS coating.

■ ASSOCIATED CONTENT

Supporting Information

The TEM images of the product for sulfidation 9 h and photoluminescence spectra of ZnO and ZnO/ZnS core/shell nanostructures obtained for different sulfidation times. This material is available free of charge via the Internet at http://pubs.acs.org/.

■ AUTHOR INFORMATION

Corresponding Author

*E-mail: chenyq63@126.com. Phone: +86-551-290-1139. Fax: +86-551-290-1362.

■ ACKNOWLEDGMENTS

This work was financially supported by the Natural Science Foundation of China (NSFC, 20803015 and 21071039).

■ REFERENCES

(1) O'Regan, B.; Grätzel, M. *Nature* **1991**, *353*, 737−740.
(2) Grätzel, M. *J. Photochem. Photobiol. C* **2003**, *4*, 145−153.
(3) Pawar, B.; Cai, G.; Hama, D.; Mane, R.; Ganesh, T.; Ghule, A.; Sharma, R.; Jadhav, K. D.; Han, S. H. *Sol. Energy Mater. Sol. Cells* **2009**, *93*, 524−527.
(4) Zheng, Y. Z.; Tao, X.; Hou, Q.; Wang, D. T.; Zhou, W. L.; Chen, J. F. *Chem. Mater.* **2011**, *23*, 3−5.
(5) Van de Lagemaat, J.; Frank, A. J. *J. Phys. Chem. B* **2001**, *105*, 11194−11205.
(6) Thavasi, V.; Renugopalakrishnan, V.; Jose, R.; Ramakrishna, S. *Mater. Sci. Eng., R* **2009**, *63*, 81−99.
(7) Xu, C. K.; Shin, P.; Cao, L. L.; Gao, D. *J. Phys. Chem. C* **2010**, *114*, 125−129.
(8) Law, M.; Greene, L. E.; Johnson, J. C.; Saykally, R.; Yang, P. *Nat. Mater.* **2005**, *4*, 455−459.
(9) Keis, K.; Bauer, C.; Boschloo, G.; Hagfeldt, A.; Westermark, K.; Rensmo, H.; Siegbahn, H. *J. Photochem. Photobiol. A* **2002**, *148*, 57−64.
(10) Yu, X. L.; Song, J. G.; Fu, Y. S.; Xie, Y.; Song, X.; Sun, J.; Du, X. W. *J. Phys. Chem. C* **2010**, *114*, 2380−2384.
(11) Li, J. H.; Zhao, D. X.; Meng, X. Q.; Zhang, Z. Z.; Zhang, J. Y.; Shen, D. Z.; Lu, Y. M.; Fan, X. W. *J. Phys. Chem. B* **2006**, *110*, 14685−14687.
(12) Meng, X. Q.; Peng, H. W.; Gai, Y. Q.; Li, J. B. *J. Phys. Chem. C* **2010**, *114*, 1467−1471.
(13) Schrier, J.; Demchenko, D.; Wang, L. W. *Nano Lett.* **2007**, *7*, 2377−2382.
(14) Liu, W.; Wang, R. M.; Wang, N. *Appl. Phys. Lett.* **2010**, *97*, 41916−41918.
(15) Bera, A.; Basak, D. *ACS Appl. Mater. Interfaces* **2010**, *2*, 408−412.
(16) Chung, J.; Myoung, J.; Oh, J.; Lim, S. *J. Phys. Chem. C* **2010**, *114*, 21360−21365.
(17) Liao, H. C.; Kuo, P. C.; Lin, C. C.; Chena, S. Y. *J. Vac. Sci. Technol., B* **2006**, *24*, 2198−2201.
(18) Greene, L.; Law, M.; Tan, D.; Montano, M.; Goldberger, J.; Somorjai, G.; Yang, P. D. *Nano Lett.* **2005**, *5*, 1231−1236.
(19) Ahmad, M.; Yan, X. X.; Zhu, J. *J. Phys. Chem. C* **2011**, *115*, 1831−1837.
(20) Kim, D. P.; Kim, C. I.; Kwon, K. H. *Thin Solid Films* **2004**, *459*, 131−136.
(21) Zaban, A.; Greenshtein, M.; Bisquert, J. *ChemPhysChem* **2003**, *4*, 860−864.
(22) Bisquert, J.; Zaban, A.; Greenshtein, M.; Mora-Sero, I. *J. Am. Chem. Soc.* **2004**, *126*, 13550−13559.
(23) Xu, C. K.; Shin, P. H.; Cao, L. L.; Wu, J. M.; Gao, D. *Chem. Mater.* **2010**, *22*, 143−148.
(24) Cheng, H. M.; Chiu, W. H.; Lee, C. H.; Tsai, S. Y.; Hsieh, W. F. *J. Phys. Chem. C* **2008**, *112*, 16359−16364.
(25) Huang, S. T.; Yang, L. *Appl. Phys. Lett.* **2011**, *98*, 93114−93116.
(26) Liu, W.; Wang, N.; Wang, R. M. *Nano Lett.* **2011**, *11*, 2983−2988.